HHS Public Access

Author manuscript

Cell Rep. Author manuscript; available in PMC 2016 September 22.

Published in final edited form as:

Cell Rep. 2015 September 22; 12(11): 1902–1914. doi:10.1016/j.celrep.2015.08.033.

TNF counterbalances the emergence of M2 tumor macrophages

Franz Kratochvill[1,2], **Geoffrey Neale**[3], **Jessica M. Haverkamp**[1,2], **Lee-Ann Van de Velde**[1,2], **Amber M. Smith**[1,2], **Daisuke Kawauchi**[5], **Justina McEvoy**[4,6], **Martine F. Roussel**[5], **Michael A. Dyer**[4], **Joseph E. Qualls**[1,2,7,*], and **Peter J. Murray**[1,2,*]

[1]Department of Infectious Diseases, St. Jude Children's Research Hospital, Memphis, TN 38105, USA

[2]Department of Immunology, St. Jude Children's Research Hospital, Memphis, TN 38105, USA

[3]Hartwell Center for Biotechnology and Bioinformatics, St. Jude Children's Research Hospital, Memphis, TN 38105, USA

[4]Department of Developmental Neurobiology, St. Jude Children's Research Hospital, Memphis, TN 38105, USA

[5]Department of Tumor Cell Biology St. Jude Children's Research Hospital, Memphis, TN 38105, USA

Abstract

Cancer is a form of non-resolving, persistent inflammation where varying numbers of tumor-associated macrophages (TAMs) infiltrate and adopt different activation states between anti-tumor M1 and pro-tumor M2 phenotypes. Here we resolve a cascade causing differential macrophage phenotypes in the tumor microenvironment. Reduction in TNF mRNA production or loss of Type I TNF receptor signaling resulted in a striking pattern of enhanced M2 mRNA expression. M2 gene expression was driven in part by IL-13 from eosinophils co-recruited with inflammatory monocytes, a pathway that was suppressed by TNF. Our data define regulatory nodes within the tumor microenvironment that balance M1 and M2 populations. Our results show macrophage polarization in cancer is dynamic and dependent on the balance between TNF and IL-13, thus providing a strategy for manipulating TAMs.

[*]Correspondence: peter.murray@stjude.org or joseph.qualls@cchmc.org.

[6]Present address: University of Arizona Cancer Center, 1515 N. Campbell Ave, Tucson, AZ 85742, USA

[7]Present address: Cincinnati Children's Hospital Medical Center, 3333 Burnet Avenue, Cincinnati, OH 45229, USA

Author contributions

FK, JEQ and PJM conceived the project and experimental design. FK and JEQ did most of the experiments. GN did the bioinformatics analysis. LVV and AMS performed key experiments to establish the tumor models and helped maintain the mouse colony. JMH performed experiments. DK, JMcE., MFR and MAD contributed key genetic tumor models, reagents and advice. PJM, FK and JEQ wrote the manuscript. All authors reviewed the manuscript.

Accession numbers

The GEO accession numbers for the microarray data are GSE59047 and GSE68817.

Introduction

Macrophages are the most abundant non-tumor cell populating cancers and their numerical presence is correlated with poor clinical outcomes (Dannenmann et al., 2013; Gajewski et al., 2013; Galon et al., 2013; Zhang et al., 2012). The large numbers of macrophages in tumors raises a simple but unanswered question: what are macrophages doing in tumors? One possibility is macrophages seed tumors to repair tissue they detect as damaged. In cancer, malignant tissue looks like 'self' thereby escaping detection by immune cells. It therefore is hardly surprising macrophages are recruited to tumors if they are performing their normal 'cleanup' functions. In doing so macrophages may aid and abet an enemy within as proposed by the Dvorak in the 'wounds that don't heal' model (Bissell and Hines, 2011; Dvorak, 1986).

Given that clinical and mouse model data frequently correlate macrophages with pro-tumor activities, several different tactics have been used to deplete or interfere with macrophage viability or recruitment including tyrosine kinase inhibitors or monoclonal antibodies targeting the colony stimulating factor 1 receptor (CSF-1R), CD11b, or antibodies targeting CCL2, a chemokine for monocyte recruitment to tumors (Ahn et al., 2010; Bonapace et al., 2014; Pyonteck et al., 2013; Ries et al., 2014). However, the anti-macrophage activity of these drugs is not limited to macrophages in tumors. Macrophages are required for normal homeostatic functions and populate all tissues of the body. Therefore, gross targeting of monocytes and/or macrophages is likely to cause toxicities in tissues dependent on macrophages such as the gut, lungs and heart (Epelman et al., 2014). Unanticipated side effects such as tumor rebound when drug therapy ceases have been reported (Bonapace et al., 2014). Macrophages are also critical for cell corpse disposal and tissue repair after chemotherapy, irradiation or surgery. In these therapies, macrophages have time-dependent pro- and anti-tumor functions (De Palma and Lewis, 2013; Klug et al., 2013; Ma et al., 2013; Nakasone et al., 2012; Predina et al., 2012). Collectively, targeting specific pro-tumor macrophage functions rather than macrophages per se could be a valuable addition to standard-of-care therapies.

Macrophages and dendritic cells are 'plastic' because their inflammatory mediator production is tailored for responsiveness to specific environmental cues (Murray and Wynn, 2011a; Wynn et al., 2013). Macrophages alter their effector and defense mechanisms across a spectrum between 'M1' pro-inflammatory phenotypes – characterized by destructive anti-intracellular pathogen free radical and inflammatory cytokine production, and 'M2' states – displayed by tissue resident macrophages, and macrophages encountering worms and fungi (Murray et al., 2014; Wynn et al., 2013). M2 macrophages express genes involved in tissue repair and resolution and have immunosuppressive and immunoregulatory properties (Murray and Wynn, 2011b). In resolving inflammation, M1 macrophages can convert into M2 macrophages to restore tissue homeostasis and integrity during and after removal of the inciting entity (Wynn et al., 2013).

By contrast to resolving inflammation, chronic cancer-associated inflammation is a non-resolving response because of the persistence of malignant cells (Biswas and Mantovani, 2010; Nathan and Ding, 2010). An emerging body of clinical and experimental evidence

links activated M1-like macrophages and cytotoxic $CD8^+$ T cells to improved overall outcomes in cancer and cancer therapy, compared to poorer outcomes in cancers harboring numerous macrophages and low numbers of $CD8^+$ T cells (Fridman et al., 2012; Gajewski et al., 2013; Predina et al., 2012). Macrophages with M2 gene expression are thought to be detrimental to anti-cancer therapies, and manipulation of their phenotype is considered key to the development of successful immunotherapies (De Palma and Lewis, 2013; Hanahan and Coussens, 2012; Qian and Pollard, 2010; Ruffell et al., 2012). Although actively debated, the mechanisms associated with macrophage polarization in cancer remain controversial. Most important is the absence of a coherent framework for understanding the signaling pathways controlling macrophage polarization, and how polarization is regulated across time and space within a tumor. Here we used a diverse range of tumor types, a systematic isolation strategy and genetic platforms to dissect the signals regulating TAM polarization. Our results elucidate how mixtures of M1 and M2 can be simultaneously present, and how these phenotypes change in tumors. We show M2 TAMs are enhanced by local amounts of IL-13, and antagonized by TNF. We found TNF is a key cytokine capable of blocking M2 gene expression in macrophages in general, and these effects of TNF on M2 genes are context dependent.

Results

Macrophage isolation procedure from diverse tumor types does not alter inflammatory gene expression

To gain insight into macrophage polarization in solid tumors we compared macrophage infiltration in diverse genetic, anatomic and orthotopic solid tumor models, including neuroblastomas, retinoblastomas, osteosarcomas, and the widely used implantable thymoma (EG7) model. Given the majority of TAMs originate from recruited $CD11b^+$ blood monocytes (Cortez-Retamozo et al., 2012; Franklin et al., 2014; Movahedi et al., 2010; Shand et al., 2014), we optimized a TAM isolation procedure based on tissue digestion and $CD11b^+$ magnetic bead isolation to capture the largest fraction of TAMs (Figure S1A). $CD11b^+$ enrichment captures all monocytes and macrophages in the tumor microenvironment, in addition to neutrophils (discussed below) and avoids plastic enrichment steps (Biswas et al., 2006), which we found caused a decrease in the expression of numerous inflammatory mRNAs following TAM adherence (Figure S1B). To determine if the isolation procedures themselves perturbed polarization-associated gene expression we developed an in vitro 3D tumor-macrophage co-culture system where bone marrow-derived macrophages are introduced into wells containing a single tumor ‘sphere’ and migrate inside (Figure S1C). We isolated the tumor-associated macrophages using the same tissue digestion and purification method described above and found few differences in M1 or M2 genes between the tumor or non-tumor macrophages. Importantly, gene expression linked to contaminating endotoxin such as TNF or IL6 was not increased by digestion (Figure S1D, E).

In $CD11b^+$ TAMs, we detected high expression of TLR2 and CD14 mRNAs while mRNAs encoding other TLRs and the IL-1R had low or undetectable expression (Figure S2A). To further determine if TAM isolation itself trigged inflammatory gene expression we

compared the CD11b$^+$ fractions from TAMs (EG7) isolated from control or MyD88-deficient mice where all TLR and IL-1R signaling (except TLR3) is ablated. Since TLR3 was not expressed in TAMs (Figure S2A), the absence of MyD88 signaling should eliminate TAM TLR/IL1R signaling and provide a sensitive readout of exogenous LPS contamination. However, the inflammatory gene signature in tumors isolated from MyD88-deficient mice revealed few differences compared to controls for most MyD88-dependent genes (Figure S2B, C). The main differences observed in MyD88-deficient CD11b$^+$ TAMs compared to controls were in mRNAs encoding members of the IL-12 family (IL-12b, IL-12a, IL-27, IL-23) and G-CSF (Figure S2B).

Collectively, we concluded our isolation procedure caused minimal experimental-derived perturbation of inflammatory gene expression. In the absence of MyD88 inflammatory gene expression stayed intact with the exception of IL-12 family members, the opposite of the conclusions drawn from in vitro adenovirus-mediated IKK manipulation (Hagemann et al., 2008). The underlying reasons for the specificity of MyD88 signaling toward such a restricted set of mRNAs in our in vivo model remains to be established, but are similar to the narrow effects of MyD88 disruption in humans (Alsina et al., 2014). Therefore, factors other than TLR or IL-1R signaling were responsible for regulating M1 gene expression in TAMs.

TAMs express M1 and M2 associated genes

We used microarray profiling and qRT-PCR of CD11b$^+$ TAMs to capture information on whether distinct tumor types influence global TAM gene expression. Regardless of their origin, we found high expression of M1-associated inflammatory genes in CD11b$^+$ TAMs (Figure 1A, S2D). The inflammatory signature of the highest expressed genes was concordant between TAMs independent of tumor type, arguing mechanisms common to the tumor microenvironment were responsible for driving the inflammatory phenotype. Closer inspection of the CD11b$^+$ TAM array data showed expression of numerous M2 signature mRNAs (Arg1, Mrc1, Chi3l3, Socs2, Ccl24) (Figure 1A). Furthermore, the CD11b$^+$ TAM fraction was ARG1$^+$ relative to separately purified tumor cells (Figure 1B). These data suggest both M1 and M2 gene expression signatures were simultaneously present within the CD11b$^+$ TAM fraction. Given reports claiming TAMs are M2 (Biswas and Mantovani, 2010) or M1 (Chittezhath et al., 2014; Franklin et al., 2014), or have more complex phenotypes (Biswas et al., 2006; Colegio et al., 2014; Elpek et al., 2014; Murray et al., 2014) we next investigated the relationship between M1-M2 TAMs in more detail.

Type 1 TNFR signaling is a central negative regulator of M2 TAMs

As discussed above, MyD88-deficient TAMs revealed few differences compared to controls for inflammatory genes (Figure S2B, C). Reasoning redundant inflammatory pathways might cooperate with MyD88 to promote the TAM signature, we focused on TNF because mRNAs encoding TNF, TNFR1 (TNFRp55, encoded by *Tnfrsf1a*) and TNFR2 (encoded by *Tnfrsf1b*) were highly expressed in TAMs based on our microarray data and TNF activates NF-κB to drive inflammation, potentially overlapping with, or compensating for, the MyD88 pathway. We therefore used mice lacking TNFR1 (called TNFR^{KO}) as a source of TAMs. Coincident with these studies we also generated mice in which type I TNF receptor,

TLR and IL-1R signaling were collectively ablated to generate a more comprehensive view of potential signaling redundancies by NF-κB-activating receptors. To do this we used TNFR1 and *Myd88*$^{\Delta H}$ TNFR^{KO} double knockout mice (called DKO). The global MyD88 knockout has multiple effects in nonhematopoietic cells (Yu et al., 2014) and we therefore generated mice lacking MyD88 in the hematopoietic compartment (called *Myd88*$^{\Delta H}$) using the Tie2-Cre deleter (El Kasmi et al., 2008). The macrophage/neutrophil-specific LysM-Cre deleter was also tested, however, the low degree of deletion of MyD88 protein in TAMs precluded the use of these mice in our experiments (Figure S2E).

TAMs lacking both MyD88 and TNFR1 showed substantial or complete reduction in most M1 inflammatory gene expression (Figure 1C) that correlated with a concomitant increase in tumor size (Figure S3A, B) that was intrinsic to macrophages as transplantation of tumors with BMDMs from control or TNFR^{KO} mice into CCR2-deficient animals (which lack the majority of TAMs) recapitulated the increases in tumor size (Figure S3C-E). TNF mRNA expression was reduced in DKO TAMs suggesting the ablation of both MyD88 and TNFR signaling disrupted feed-forward inflammatory loops driving M1 gene expression via TNF (Figure 1D). Thus, TLR/IL-1R and TNF signaling collectively enforced a cooperative pro-inflammatory pathway responsible for the M1-like TAM signature, and these data likely accounted for the limited phenotype of the MyD88-deficient mice; TNF signaling is redundant with TLR/IL-1R signaling in TAMs.

By contrast to the reduction in M1 gene expression in DKO mice, M2 gene expression in TAMs from TNFR^{KO}, DKO and to a certain extent from *Myd88*$^{\Delta H}$ mice showed a remarkable signature (Figure 1E). TAMs isolated from DKO mice showed increased production of M2 associated mRNAs suggesting that MyD88 and TNF signaling collectively masked or actively repressed M2 gene expression. In *MyD88*$^{\Delta H}$ TAMs, the TNF mRNA was amongst the strongest reduced transcripts. We therefore hypothesize the effects of MyD88 deletion in TAMs on M2 associated genes expression rely on reduced signaling downstream TNFR1 similar to TNFR^{KO} TAMs.

M2 gene expression is enriched in CD11b^{+}, Ly6C^{-}, MHCII^{+} TAMs from TNFR^{KO} mice

An issue stemming from the above experiments concerned which cells in the tumor microenvironment were expressing the M2 markers. To address this we noted many MyD88-dependent genes in the CD11b^{+} fraction were enriched in the Ly6G^{+} neutrophil fraction (Figure S3F). These data prompted us to modify our TAM isolation procedure (Figure 2A, B) to more specifically isolate different TAM fractions (Kratochvill et al., 2015). We built upon methodologies (Movahedi et al., 2010; O'Sullivan et al., 2012) where the CD11b^{+} fraction was sub-divided into four populations: neutrophils (Ly6G^{+}, CD11b^{+}), the TAMs directly descended from blood monocytes called TAM-A (CD11b^{+}, Ly6C^{hi}, MHCII^{-}), TAM-B (CD11b^{+}, Ly6C^{+}, MHCII^{+}) and TAM-C (CD11b^{+}, Ly6C^{-}, MHCII^{+}). TAM-A, -B and -C originated from monocytes because each of these cells was absent in *Ccr2*$^{-/-}$ mice (Figure 2A) (Cortez-Retamozo et al., 2012; Franklin et al., 2014; Shand et al., 2014). Furthermore, results from tracing relationships between monocytes and their progeny suggests ‘mature’ TAM-C are descended from TAM-A (Movahedi et al., 2010), in a process similar to other inflammatory models where local macrophages originate from blood

monocytes seeding an inflammatory site (Bain and Mowat, 2014; Bain et al., 2013). Furthermore, the $CD11b^+$ population contains cells consistent with their identity as eosinophils (Eos, discussed below) distinguished from monocytes by the degree of Ly6C expression (Figure 2A, B). Consistent with other data showing macrophage cell surface phenotypes change with maturation from monocytes (Movahedi et al., 2010; O'Sullivan et al., 2012), we found increased F4/80 and CX3CR1 expression on mature TAM-B and TAM-C relative to the monocyte-rich TAM-A fraction (Figure 2C).

Coincident with our flow cytometry protocol, we used orthotopic tumor models as a reproducible experimental standard that can be transplanted into any mouse on a C57BL/6 background (EG7, Lewis lung carcinoma, and B16 melanoma). When we compared the $CD11b^+$ populations in each model, a gradient of non-monocytic $Ly6C^+$ infiltration was observed. EG7 tumors had high numbers of non-monocytic $Ly6C^+$while B16 tumors were devoid of these cells (Figure 2D). As described later, this heterogeneity provided a platform to test the contribution of eosinophils to TAM polarization phenotypes. We therefore sorted the TAM-A and TAM-C fractions from EG7-bearing mice and subjected each fraction to microarray analysis. We found that the expression of nearly all M2 marker mRNAs were (i) enriched in the TAM-C fraction relative to TAM-A, and (ii) increased in the absence of type I TNFR signaling (Figure 2E). These data suggest TNF is an *in vivo* repressor of M2 signaling in TAMs.

TNF blocks STAT6-dependent M2 gene expression in a gene-specific manner

We next asked if TNF was a general inhibitor of M2 gene expression (Figure 3A). We generated bone marrow-derived macrophages (BMDMs) with recombinant CSF-1 and stimulated them with IL-4 and IL-13 to induce M2 gene expression via STAT6, with or without recombinant TNF. We measured M2 gene expression by qRT-PCR and found three patterns (Figure 3A, B, C). First, mRNAs encoding Retnla (also called FIZZ1), Mgl2 and Mrc1 (mannose receptor) were induced by IL-4 and IL-13 as expected, but repressed by TNF (Figure 3A). Arg1 mRNA was also induced by IL-4 and IL-13 as expected but not blocked by TNF (Figure 3B). The final group of mRNAs encoded the M2 chemokines CCL17 and CCL22, which were induced by TNF but not by IL-4 and IL-13; the opposite phenotype to TAMs where expression of each mRNA is enhanced in the absence of TNFR1 signaling (Figure 1E, 2E). When viewed collectively these data showed the negative effects of TNF on M2 gene expression we observed in the tumor microenvironment can only in part be translated to in vitro experiments using BMDMs. Importantly, TNF blocked M2 expression in a gene- and macrophage-type specific way. The latter point prompted us to return to investigate in more detail the signaling events that established the M2 phenotype within the tumor microenvironment.

STAT6 is required for TAM M2 gene expression

Recent results showed lactate and hypoxia are important factors in amplifying M2-associated gene expression, especially *Arg1* (Colegio et al., 2014; El Kasmi et al., 2014). However, IL-4 and IL-13, via STAT6 phosphorylation, are widely accepted as the major drivers of M2 gene expression. We found TAM-A and TAM-C from EG7 TAMs expressed the IL-4Rα and IL-13Rα (Figure 3D) consistent with the ability of these cells to activate

STAT6. We used the orthotopic transplant system in *Stat6*$^{-/-}$ mice on a pure C57BL/6 background and generated TAM fractions. We found overall M2 gene expression for six targets and expression of PD-L2 (Huber et al., 2010), was reduced or eliminated in the absence of STAT6 (Figure 3E and F). However, these data also allowed us to test the STAT6-independent expression of individual genes. Consistent with recent data (Colegio et al., 2014), Arg1 mRNA expression was partially affected by the loss of STAT6, indicating other pathways regulate Arg1, while mRNAs encoding Retnla and Ccl24 were substantially reduced (Figure S4A). Importantly, the amounts of surface IL-4Rα or IL-13Rα were unaffected by genetic perturbation of the STAT6 or TNFR pathways (Figure 3G). These data are consistent with a model where multiple factors collaborate to provide an M2 permissive environment; lactate/hypoxia are likely one signal collaborating with STAT6, but work in a gene-specific way (Colegio et al., 2014; El Kasmi et al., 2014).

IL-13 amplifies M2 TAMs and is blocked by TNF

Given our data showed an important contribution of IL-4 and IL-13-activated STAT6 to TAM M2 gene expression we next asked whether we could detect IL-13 or IL-4 in the tumor environment. We found elevated amounts of IL-13 in bulk TAMs isolated from TNFR^{KO} mice raising the possibility that IL-13 expression was suppressed by TLR and/or TNF signaling (Figure 4A). IL-4 and IL-13 are produced by many immune cells including T cells, ILCs, neutrophils and even macrophages under certain conditions. Unlike recent findings showing neutrophils are a central source of IL-13 in helminth infections (Chen et al., 2014), we could not detect IL-13 in tumor infiltrating Ly6G^{+} neutrophils (Figure 4B). Similarly, we found T cell numbers in orthotopic tumors were very low and unchanged in the TNFR^{KO} mice, suggesting T cells were not a major source of IL-13 in our models (Figure S4B-F). However, IL-13 mRNA expression was enriched in non-monocytic CD11b^{+} Ly6C^{+} cells from TNFR^{KO} mice with characteristics of eosinophils (Lee et al., 2012) (Figure 4B, C). The eosinophil-like cells expressed variable amounts of SiglecF and had the cytological appearance of eosinophils (Figure 4C, D). However, they did not express CCR3, an eosinophil and red pulp macrophage marker as defined by the ImmGen database, which may be down regulated in the tumor microenvironment. These cells are referred to hereafter as eosinophils. Neutralization of IL-13 with a monoclonal antibody (mAb) in EG7-bearing TNFR^{KO} mice showed partial reduction of M2 gene expression, consistent with the idea that local IL-13 is required in part to increase TAM M2 polarization (Figure 4E).

These data suggested TNF signaling negatively regulates two steps in the tumor microenvironment. First, TNF directly blocked specific sets of M2 genes. Second, TNF suppressed IL-13 expression from eosinophils, and thus prevented production of a key M2-activating cytokine; the net effect was local reduction in M2 gene expression. If this model is valid, then we should be able to correlate eosinophil numbers in tumors with M2 gene expression. To test this prediction, we used the orthotopic transplant system where EG7, LLC and B16 tumors were infiltrated with different amounts of eosinophils, such that EG7 had the most and B16 tumors the least (Figure 2D, 5A). Consistent with our model, the number of eosinophils correlated with the amount of IL-13 mRNA detected in the different tumor models in TNFR^{KO} mice (Figure 5B). When we analyzed gene expression in each tumor, a correlation in M2 expression from EG7>LLC>B16 was observed in the TNFR-

deficient mice (Figure 5C). These data therefore define, in an in vivo model system, that TNF signaling is a negative regulator of both IL-13 production and responsiveness of macrophages to IL-13.

Anti-TNF drugs have been successfully used for chronic inflammation for two decades. The mechanism of action of anti-TNF drugs is to block TNF, limiting feed-forward inflammation. However, based on our data, a linked mechanism could be the promotion of M2 macrophages. To test this hypothesis in cancer we used Etanercept, a soluble TNFR that partially limits TNF bioavailability. Administration of Etanercept to mice bearing EG7 tumors caused a relative increase in IL-13 as well as M2 gene expression in $CD11b^{+}$ TAMs that did not reach the magnitude of the effect seen in the complete $TNFR^{KO}$ mice as expected based on previous experiments comparing Etanercept and potent antibody-based TNF blockers (Vos et al., 2012) (Figure 6A, B). Consistent with data showing Arg1 gene expression is regulated by via multiple pathways, Arg1 mRNA was not increased by Etanercept treatment (Figure 6C). Therefore, TNF inhibition is linked to the promotion of M2 macrophages, which may contribute to the salutary effects of anti-TNF drugs in colitis and rheumatoid arthritis, but may also promote a tumor-permissive M2 environment in cancer.

Discussion

Our experiments provide a conceptual framework for explaining why both M1 and M2 TAMs have been observed in cancer: the quantity of macrophages at either end of the polarization spectrum depends on the balance between IL-13 (and possibly IL-4) delivery by eosinophils, and the overall amount of TLR, IL-1R and TNFR signaling. Therefore, we predict cancers associated with high amounts of endogenous commensal- and pathogen-derived molecules, DAMPs and TNF such as colon cancer, will trend to the M1 end of the spectrum because the STAT6-dependent M2 response will be suppressed. Conversely, we predict tumors with low relative inflammation such as at sterile sites like breast and head and neck tumors, or developmental tumors of childhood, will have higher relative numbers of M2 macrophages because the TNF: M2 balance shifts in favor of M2 TAMs. This balance is likely further controlled by temporal and spatial variables within the microenvironment.

The key finding of our work is that TNF negatively regulates M2 gene expression both in vivo and in vitro. We established TNF did not inhibit all M2 gene expression. Instead, TNF targeted subsets of genes. These data argue for a model where downstream signals from the type I TNFR such as NF-κB, act in a gene specific way. Our data can be used to explain phenotypes of knockout mice where unanticipated polarization switching was observed but could be correlated with local TNF production. For example, CD14-deficient mice have greatly enhanced M2-driven granulomatous response to schistosome eggs trapped in the liver. In these granulomas, macrophages express high amounts of M2 genes Retnla, Arg1 and Chi3l3 expression relative to controls (Tundup et al., 2014). One explanation for the phenotype is loss of CD14, an essential surface component of TLR signaling, will lead to defects in local TNF production and enhanced M2 responses. Another example of chronic inflammation linked to the inverse balance between TNF and M2 macrophages is obesity. In

lean adipose tissue, M2-like tissue resident macrophages interdigitate between fat cells, while in obesity, excess fat suppresses M2 macrophages and is associated with increased TNF (Lumeng et al., 2007; Weisberg et al., 2003; Xu et al., 2003). However, when TLR4 signaling is genetically ablated in obesity, M2 associated macrophage genes increase, and this phenotype paralleled a decline in TNF (Orr et al., 2012). Therefore, a general prediction from our studies is many inflammation-linked polarization phenotypes might be dictated by an inverse relationship between TNF and signals driving M2 polarization (IL-4, IL-13); increased TNF will block M2 polarization in a gene-specific way, depending on quantity, time and spatial availability. The conceptual advance made here to inversely link M2 polarization and TNF may also help explain why cytotoxic therapy is linked to M1 macrophages as the necrotic and apoptotic death of large numbers of tumor cells releases DAMPs (Klug et al., 2013), which through local TNF generation, will suppress IL-13 and IL-4 from eosinophils and thus also suppress STAT6-dependent M2 TAMs. Finally, we suggest anti-TNF drugs might also work through the combined effects of suppressing a pro-inflammatory signal that concomitantly causes a rise in M2 macrophages. Indeed, anti-TNF drugs promote changes in macrophage phenotype, and this effect is proportional to TNF neutralization (Vos et al., 2012; Vos et al., 2011). We used Etanercept, a soluble TNFR, which was noted to have the weakest effect of macrophage phenotypic changes. Our in vivo data confirmed this finding, as Etanercept caused increases in TAM M2 gene expression, which were less than that observed in the complete TNFR1-deficient mice. Therefore, we consider an important direction stemming from our work will be to reconsider the mechanistic actions of TNF blockers. For example, anti-TNF therapy causes tuberculosis reactivation, a phenotype attributed to removal of TNF (Flynn et al., 1995). However, because M2 macrophages are permissive to TB (Potian et al., 2011), we predict part of the reason anti-TNF drugs are contraindicated for TB infected patients is linked to elevations of M2 macrophages.

A previous study using an ovarian cancer model claimed NF-κB signaling was required for maintaining the expression of M2 genes (Hagemann et al., 2008). These results are difficult to interpret for several reasons. NF-κB signaling is necessary for most inflammatory gene expression. In Hagemann et al, inhibition of NF-κB by manipulating IKKβ caused increases in IL-12p40 and iNOS expression (Hagemann et al., 2008), the opposite of what one would expect, as expression of both genes requires contributions from NF-κB complexes for optimal expression (Farlik et al., 2010; Sanjabi et al., 2000; Sen and Smale, 2010; Zhou et al., 2004). In our in vivo studies, IL-12p40 expression is dependent on MyD88 in TAMs residing in the tumor microenvironment arguing for a positive role of NF-κB activation downstream of TLR signaling. The conclusions drawn by Hagemann et al. derived from an experimental system where adenoviruses were used to transfer dominant negative versions of IKKβ, or Cre recombinase into CSF-1 generated bone marrow-derived macrophages. As the effects of viral infection in the absence of functional NF-κB signaling in the experimental arms were unaccounted for, the claims of this study remain difficult to interpret and differ from most other findings in the field.

Our data clearly show eosinophil-derived IL-13 is one factor provoking M2 polarization. Therefore, local IL-13 will enhance M2 polarization, depending on how much TNF is present. IL-4 may also be a key factor in TAM M2 polarization, but we found IL-4

expression difficult to reliably detect, consistent with observations made in other systems, and with different IL-4 reporter mice (Liang et al., 2012). Our data are consistent with recent studies in helminth infections showing neutrophils are the source of M2-enhancing cytokines, and that eosinophils produce IL-4 and IL-13 in beige fat-associated macrophages (Chen et al., 2014; Qiu et al., 2014). One unexpected facet of our data was the inhibitory effect of TNF on IL-13 production from eosinophils, as the loss of type I TNF signaling greatly enhanced eosinophil IL-13 production. Therefore, an eosinophil-intrinsic signaling pathway from the TNFR blocks IL-13. Indeed, a recent study has shown eosinophils have potent anti-tumor properties when activated and co-transferred with cytotoxic T cells (Carretero et al., 2015). In this study, the eosinophils were pre-treated with TNF and IFN-γ and co-transferred with activated OT1 T cells, which can make TNF. Therefore, understanding the balance of signals that control TNF, IL-13, eosinophils and TAMs may be important in understanding and modulating inflammation in addition to the potential for rational manipulation of macrophage polarization in the tumor microenvironment.

Experimental Procedures

Mice

C57Bl/6, *Myd88*$^{flox/flox}$, *Stat6*$^{-/-}$, B6.Cg-*Tg*(*Tek-cre*)^{1Ywa} (Tie2-Cre), *Ccr2*$^{-/-}$, *Cx3cr1*^{GFP} and *Lyz2*$^{tm1(cre)Ifo}$/J (LysM-Cre) mice were obtained from Jackson Laboratories (Bar Harbor, ME). TNFR1 knockout mice (*Tnfrsf1a*$^{-/-}$) were a gift from V. Redecke (St. Jude Children's Research Hospital, Memphis, TN). *Myd88*$^{-/-}$ mice were obtained from D. Green (St. Jude Children's Research Hospital, Memphis, TN), and were originally a gift from S. Akira (Osaka University, Osaka, Japan). *Arg1*$^{flox/flox}$ mice have been described elsewhere and were crossed to Tie2-Cre mice (El Kasmi et al., 2008). Littermate controls that were Cre negative or positive were used. The above mentioned mouse lines were crossed to a pure C57Bl/6 background (>10 generations) in house or as supplied from Jackson Laboratories. C57Bl/6 control animals were breed and housed in the same rooms at St. Jude Children's Research Hospital. Where intercrossing was performed, littermate controls were used where feasible. All mouse breeding, husbandry and tumor models were performed according to established guidelines for laboratory animal use.. Th-MYCN transgenic (Weiss et al., 1997), *Chx10*-Cre, *Rb*$^{flox/flox}$; *p107*$^{-/-}$; *p130*$^{flox/flox}$ and *Mdmx*-tg; *Rb*$^{flox/flox}$; *p107*$^{-/-}$; *Chx10*-Cre mice were used as sources of retinoblastomas and *Rb*$^{flox/flox}$; *p53*$^{flox/flox}$; *Osx*-Cre^{+} mice were used to generate osteosarcomas. All mice used in this study were co-housed by sex and were bred and used within the Animal Resource Center according to protocols approved by the IACUC at St. Jude Children's Research Hospital.

Tumor models – in vivo

Glioma (G): Gliomas were engineered from granule neural progenitors purified from cerebella of *Tp53*$^{-/-}$, *Cdkn2c*$^{-/-}$, *Math1-GFP* 5-7 days old pups, transduced with retroviruses expressing an HER2/Neu mutant ERBB2 V695A and the red fluorescent protein dsRed (MSCVERBB2V695A-IRES-dsRed). 1×10^3 GFP-RFP double-positive cells were implanted in the cortices of CD1 nude mice (Kawauchi et al., 2012) for 69-77 days. 3×10^6 tumor cells from dissociated gliomas were injected subcutaneously into the flank of recipient C57BL/6 mice for TAM isolation. Thymoma (T): EG7 lymphoma line originating from the thymus

(EL4), stably expressing OVA protein. 3×10^6 EG7 cells, grown *in vitro*, were injected subcutaneously into the flank of recipient mice. Gliomas and thymomas were harvested from mice between 1.5 and 2 weeks post-transplant. Neuroblastoma (N): Spontaneous neuroblastomas detected by ultrasound were collected from the peritoneum of Th-MYCN transgenic (tg) mice. Retinoblastoma (R): Spontaneous retinoblastomas were collected behind the eye from either *Rb*$^{flox/flox}$; *p107*$^{-/-}$; *Chx10*-Cre, and *MDMX*-tg; *Rb*$^{flox/flox}$; *p107*$^{-/-}$; *Chx10*-Cre mice. Osteosarcoma (O): Spontaneous osteosarcomas were collected from Rb$^{flox/flox}$; *p53*$^{flox/flox}$; *Osx*-Cre^{+} mice. LLC and B16 tumor models were used as described (Haverkamp et al., 2014).

Media and Reagents

Tumor digestion media (TDM): 5 mg DNase I (Worthington), 12.5 mg collagenase P (Roche), 12.5 mg collagenase/dispase (Roche), 100 μl B27 (Invitrogen), 50 μl N2 (Invitrogen), made to 5 ml with Neural Basal medium (Invitrogen), followed by 0.22 μm filter sterilization. *DNase solution (DS)*: 7.5 mg DNase I (Worthington), 120 μl 45% glucose solution (Sigma-Aldrich), up to 15 ml with 1× Basal Medium Eagle media (Invitrogen), followed by 0.22 μm filter sterilization. *Percoll solution*: Percoll (Sigma-Aldrich) was adjusted to a final pH of 7.4 followed by 0.22 μm filter sterilization. 35% percoll (25 ml 4× PBS-EDTA, 35 ml percoll, 40 ml water) and 60% percoll (25 ml 4× PBS-EDTA, 60 ml percoll, 15 ml water, 300 μl 0.4 % trypan blue (Invitrogen) stocks were prepared and stored at 4°C. *Cytokines*: IL-4, TNF, IFN-γ (all eBioscience), IL-13 (Peprotech) and LPS (Sigma-Aldrich) were used at 10 ng/ml, 10ng/ml, 2 ng/ml, 40 ng/ml or 100 ng/ml, respectively. Anti-mouse IL-13 antibody and IgG1 control (Clone MOPC-21) were provided by Genentech, Inc. and Bio X Cell, respectively.

Tumor-associated macrophage isolation

Solid tumors were excised and minced using a scalpel. 5 ml of fresh TDM was added, transferred to a 50 ml conical tube, and incubated for 20 minutes shaking at 37°C. Tumor fragments were dissociated with a 10 ml pipet, and passed through a 70 μm strainer. To collect loosely attached cells, the strainer was then washed with 10 mls PBS. Tumor cells were centrifuged for 5 minutes at 300g, 4°C, and the supernatant was aspirated. Cells were resuspened in 1 ml fresh DS. Following resuspension, 4 ml PBS was added and cells were overlaid on a 35%/60% percoll gradient. Percoll gradients with cells were centrifuged for 20 minutes at 2000g, 4° C with the brakes disengaged. Tumor cells and macrophages were collected from the 35%/60% interphase, transferred to a 50 ml conical tube containing 10 mls PBS, and centrifuged for 5 minutes at 300g, 4°C. For RNA preparation of TAMs or TAM populations after cell sorting, cells were resuspended in MACS buffer with 10% normal mouse serum for blocking, and TAMs were collected by CD11b purification using Miltenyi magnetic beads. CD11b^{+} and CD11b^{-} fractions were analyzed by flow cytometry and/or cytospin.

Flow cytometry

Cells were resuspended in 200 μl FACS buffer (PBS with 5% bovine calf serum) and placed on ice for 15 minutes to block. Cells were incubated with fluorescently labeled antibodies on

ice in the dark for 20 minutes then washed with PBS, centrifuged at 500×g for 5 minutes, resuspended in 200 μl FACS buffer, and evaluated on a FACSCanto (Becton Dickenson) flow cytometer. Cell death was determined using an Annexin V Apoptosis Detection Kit I (BD Pharmingen). Data were further analyzed using FlowJo software (Tree Star, Inc.).

RNA isolation and qRT-PCR analysis

RNA was collected from TAMs and other cells using Trizol (Invitrogen), according to the manufacturer's protocol. cDNA was synthesized using SuperScript II reverse transcriptase (Invitrogen), and analyzed by qRT-PCR using the primer pairs listed in Supplemental Information. All values were normalized to GAPDH.

Anti-IL-13 antibody treatment

200 μg anti-IL-13 antibody or IgG1 control were injected i.v. per mouse bearing EG7 thymomas 6 days before tumor harvest.

Etanercept treatment

EG7 tumor bearing mice received a daily dose of 0.060 mg/mouse Etanercept (Enbrel) or PBS as control by subcutaneous injection starting 5 days after implantation of the EG7 cells until tumor harvest on day 11.

Statistics

Data indicate the mean +/− SEM of representative experiments. Statistical significance was determined by a two-tailed Student's t test or One-way Anova followed by Bonferroni Post Test where indicated in the figure legends using Graphpad Prism5 justified according to the normality and variance of the distribution (*$p < 0.05$, **$p < 0.01$, ***$p < 0.001$). Sample size for adequate power was estimated using preliminary studies.

Supplementary Material

Refer to Web version on PubMed Central for supplementary material.

Acknowledgments

We thank Melissa Johnson and Chris Calabrese for animal imaging, Genentech and Lawren Wu for the gift of anti-IL-13 antibodies, and Richard Gilbertson for the gift of the ERBB2 V695A mutant plasmid. This work was supported by NIH grants CA189990 (PJM), CA096832 (MFR) and CA138064 (JEQ); by Alex's Lemonade Stand Foundation and the Hartwell Foundation (PJM), Cancer Center Core Grant P30 CA21765 (PJM, MFR), the Austrian Science Fund J3309-B19 (FK), the Anderson Fellowship (DK) and the American Lebanese Syrian Associated Charities of St. Jude Children's Research Hospital.

References

Ahn GO, Tseng D, Liao CH, Dorie MJ, Czechowicz A, Brown JM. Inhibition of Mac-1 (CD11b/CD18) enhances tumor response to radiation by reducing myeloid cell recruitment. Proc Natl Acad USA. 2010; 107:8363–8368.

Alsina L, Israelsson E, Altman MC, Dang KK, Ghandil P, Israel L, von Bernuth H, Baldwin N, Qin H, Jin Z, et al. A narrow repertoire of transcriptional modules responsive to pyogenic bacteria is impaired in patients carrying loss-of-function mutations in MYD88 or IRAK4. Nat Immunol. 2014; 15:1134–1142. [PubMed: 25344726]

Bain CC, Mowat AM. Macrophages in intestinal homeostasis and inflammation. Immunol Rev. 2014; 260:102–117. [PubMed: 24942685]

Bain CC, Scott CL, Uronen-Hansson H, Gudjonsson S, Jansson O, Grip O, Guilliams M, Malissen B, Agace WW, Mowat AM. Resident and pro-inflammatory macrophages in the colon represent alternative context-dependent fates of the same Ly6Chi monocyte precursors. Mucosal Immunol. 2013; 6:498–510. [PubMed: 22990622]

Bissell MJ, Hines WC. Why don't we get more cancer? A proposed role of the microenvironment in restraining cancer progression. Nat Med. 2011; 17:320–329. [PubMed: 21383745]

Biswas SK, Gangi L, Paul S, Schioppa T, Saccani A, Sironi M, Bottazzi B, Doni A, Vincenzo B, Pasqualini F, et al. A distinct and unique transcriptional program expressed by tumor-associated macrophages (defective NF-kappaB and enhanced IRF-3/STAT1 activation). Blood. 2006; 107:2112–2122. [PubMed: 16269622]

Biswas SK, Mantovani A. Macrophage plasticity and interaction with lymphocyte subsets: cancer as a paradigm. Nature Immunol. 2010; 11:889–896. [PubMed: 20856220]

Bonapace L, Coissieux MM, Wyckoff J, Mertz KD, Varga Z, Junt T, Bentires-Alj M. Cessation of CCL2 inhibition accelerates breast cancer metastasis by promoting angiogenesis. Nature. 2014; 515:130–133. [PubMed: 25337873]

Carretero R, Sektioglu IM, Garbi N, Salgado OC, Beckhove P, Hammerling GJ. Eosinophils orchestrate cancer rejection by normalizing tumor vessels and enhancing infiltration of CD8(+) T cells. Nat Immunol. 2015; 16:609–617. [PubMed: 25915731]

Chen F, Wu W, Millman A, Craft JF, Chen E, Patel N, Boucher JL, Urban JF Jr. Kim CC, Gause WC. Neutrophils prime a long-lived effector macrophage phenotype that mediates accelerated helminth expulsion. Nat Immunol. 2014; 15:938–946. [PubMed: 25173346]

Chittezhath M, Dhillon MK, Lim JY, Laoui D, Shalova IN, Teo YL, Chen J, Kamaraj R, Raman L, Lum J, et al. Molecular Profiling Reveals a Tumor-Promoting Phenotype of Monocytes and Macrophages in Human Cancer Progression. Immunity. 2014; 41:815–829. [PubMed: 25453823]

Colegio OR, Chu NQ, Szabo AL, Chu T, Rhebergen AM, Jairam V, Cyrus N, Brokowski CE, Eisenbarth SC, Phillips GM, et al. Functional polarization of tumour-associated macrophages by tumour-derived lactic acid. Nature. 2014; 513:559–563. [PubMed: 25043024]

Cortez-Retamozo V, Etzrodt M, Newton A, Rauch PJ, Chudnovskiy A, Berger C, Ryan RJ, Iwamoto Y, Marinelli B, Gorbatov R, et al. Origins of tumor-associated macrophages and neutrophils. Proc Natl Acad Sci U S A. 2012; 109:2491–2496. [PubMed: 22308361]

Dannenmann SR, Thielicke J, Stockli M, Matter C, von Boehmer L, Cecconi V, Hermanns T, Hefermehl L, Schraml P, Moch H, et al. Tumor-associated macrophages subvert T-cell function and correlate with reduced survival clear cell renal cell carcinoma. Oncoimmunology. 2013; 2:e23562. [PubMed: 23687622]

De Palma M, Lewis CE. Macrophage regulation of tumor responses to anticancer therapies. Cancer Cell. 2013; 23:277–286. [PubMed: 23518347]

Dvorak HF. Tumors: wounds that do not heal. Similarities between tumor stroma generation and wound healing. N Engl J Med. 1986; 315:1650–1659. [PubMed: 3537791]

El Kasmi KC, Pugliese SC, Riddle SR, Poth JM, Anderson AL, Frid MG, Li M, Pullamsetti SS, Savai R, Nagel MA, et al. Adventitial fibroblasts induce a distinct proinflammatory/profibrotic macrophage phenotype in pulmonary hypertension. J Immunol. 2014; 193:597–609. [PubMed: 24928992]

El Kasmi KC, Qualls JE, Pesce JT, Smith AM, Thompson RW, Henao-Tamayo M, Basaraba RJ, Konig T, Schleicher U, Koo MS, et al. Toll-like receptor-induced arginase 1 in macrophages thwarts effective immunity against intracellular pathogens. Nature Immunol. 2008; 9:1399–1406. [PubMed: 18978793]

Elpek KG, Cremasco V, Shen H, Harvey CJ, Wucherpfennig KW, Goldstein DR, Monach PA, Turley SJ. The Tumor Microenvironment Shapes Lineage, Transcriptional, and Functional Diversity of Infiltrating Myeloid Cells. Cancer Immunol Res. 2014; 2:655–667. [PubMed: 24801837]

Epelman S, Lavine KJ, Randolph GJ. Origin and functions of tissue macrophages. Immunity. 2014; 41:21–35. [PubMed: 25035951]

Farlik M, Reutterer B, Schindler C, Greten F, Vogl C, Muller M, Decker T. Nonconventional initiation complex assembly by STAT and NF-kappaB transcription factors regulates nitric oxide synthase expression. Immunity. 2010; 33:25–34. [PubMed: 20637660]

Flynn JL, Goldstein MM, Chan J, Triebold KJ, Pfeffer K, Lowenstein CJ, Schreiber R, Mak TW, Bloom BR. Tumor necrosis factor-alpha is required in the protective immune response against Mycobacterium tuberculosis in mice. Immunity. 1995; 2:561–572. [PubMed: 7540941]

Franklin RA, Liao W, Sarkar A, Kim MV, Bivona MR, Liu K, Pamer EG, Li MO. The cellular and molecular origin of tumor-associated macrophages. Science. 2014; 344:921–925. [PubMed: 24812208]

Fridman WH, Pages F, Sautes-Fridman C, Galon J. The immune contexture in human tumours: impact on clinical outcome. Nat Rev Cancer. 2012; 12:298–306. [PubMed: 22419253]

Gajewski TF, Schreiber H, Fu YX. Innate and adaptive immune cells in the tumor microenvironment. Nat Immunol. 2013; 14:1014–1022. [PubMed: 24048123]

Galon J, Angell HK, Bedognetti D, Marincola FM. The continuum of cancer immunosurveillance: prognostic, predictive, and mechanistic signatures. Immunity. 2013; 39:11–26. [PubMed: 23890060]

Hagemann T, Lawrence T, McNeish I, Charles KA, Kulbe H, Thompson RG, Robinson SC, Balkwill FR. “Re-educating” tumor-associated macrophages by targeting NF-kappaB. J Exp Med. 2008; 205:1261–1268. [PubMed: 18490490]

Hanahan D, Coussens LM. Accessories to the crime: functions of cells recruited to the tumor microenvironment. Cancer Cell. 2012; 21:309–322. [PubMed: 22439926]

Haverkamp JM, Smith AM, Weinlich R, Dillon CP, Qualls JE, Neale G, Koss B, Kim Y, Bronte V, Herold MJ, et al. Myeloid-derived suppressor activity is mediated by monocytic lineages maintained by continuous inhibition of extrinsic and intrinsic death pathways. Immunity. 2014; 41:947–959. [PubMed: 25500368]

Huber S, Hoffmann R, Muskens F, Voehringer D. Alternatively activated macrophages inhibit T-cell proliferation by Stat6-dependent expression of PD-L2. Blood. 2010; 116:3311–3320. [PubMed: 20625006]

Kawauchi D, Robinson G, Uziel T, Gibson P, Rehg J, Gao C, Finkelstein D, Qu C, Pounds S, Ellison DW, et al. A mouse model of the most aggressive subgroup of human medulloblastoma. Cancer Cell. 2012; 21:168–180. [PubMed: 22340591]

Klug F, Prakash H, Huber PE, Seibel T, Bender N, Halama N, Pfirschke C, Voss RH, Timke C, Umansky L, et al. Low-dose irradiation programs macrophage differentiation to an iNOS(+)/M1 phenotype that orchestrates effective T cell immunotherapy. Cancer Cell. 2013; 24:589–602. [PubMed: 24209604]

Kratochvill F, Gratz N, Qualls JE, Van De Velde LA, Chi H, Kovarik P, Murray PJ. Tristetraprolin Limits Inflammatory Cytokine Production in Tumor-Associated Macrophages in an mRNA Decay-Independent Manner. Cancer Res. 2015 In press. doi: 10.1158/0008-5472.CAN-15-0205.

Lee JJ, Jacobsen EA, Ochkur SI, McGarry MP, Condjella RM, Doyle AD, Luo H, Zellner KR, Protheroe CA, Willetts L, et al. Human versus mouse eosinophils: “that which we call an eosinophil, by any other name would stain as red”. J Allergy Clin Immunol. 2012; 130:572–584. [PubMed: 22935586]

Liang HE, Reinhardt RL, Bando JK, Sullivan BM, Ho IC, Locksley RM. Divergent expression patterns of IL-4 and IL-13 define unique functions in allergic immunity. Nat Immunol. 2012; 13:58–66. [PubMed: 22138715]

Lumeng CN, Bodzin JL, Saltiel AR. Obesity induces a phenotypic switch in adipose tissue macrophage polarization. J Clin Invest. 2007; 117:175–184. [PubMed: 17200717]

Ma Y, Adjemian S, Mattarollo SR, Yamazaki T, Aymeric L, Yang H, Portela Catani JP, Hannani D, Duret H, Steegh K, et al. Anticancer chemotherapy-induced intratumoral recruitment and differentiation of antigen-presenting cells. Immunity. 2013; 38:729–741. [PubMed: 23562161]

Movahedi K, Laoui D, Gysemans C, Baeten M, Stange G, Van den Bossche J, Mack M, Pipeleers D, In't Veld P, De Baetselier P, et al. Different tumor microenvironments contain functionally distinct subsets of macrophages derived from Ly6C(high) monocytes. Cancer Res. 2010; 70:5728–5739. [PubMed: 20570887]

Murray PJ, Allen JE, Biswas SK, Fisher EA, Gilroy DW, Goerdt S, Gordon S, Hamilton JA, Ivashkiv LB, Lawrence T, et al. Macrophage Activation and Polarization: Nomenclature and Experimental Guidelines. Immunity. 2014; 41:14–20. [PubMed: 25035950]

Murray PJ, Wynn TA. Obstacles and opportunities for understanding macrophage polarization. J leukocyte biol. 2011a; 89:557–563. [PubMed: 21248152]

Murray PJ, Wynn TA. Protective and pathogenic functions of macrophage subsets. Nature reviews Immunology. 2011b; 11:723–737.

Nakasone ES, Askautrud HA, Kees T, Park JH, Plaks V, Ewald AJ, Fein M, Rasch MG, Tan YX, Qiu J, et al. Imaging tumor-stroma interactions during chemotherapy reveals contributions of the microenvironment to resistance. Cancer Cell. 2012; 21:488–503. [PubMed: 22516258]

Nathan C, Ding A. Nonresolving inflammation. Cell. 2010; 140:871–882. [PubMed: 20303877]

O'Sullivan T, Saddawi-Konefka R, Vermi W, Koebel CM, Arthur C, White JM, Uppaluri R, Andrews DM, Ngiow SF, Teng MW, et al. Cancer immunoediting by the innate immune system in the absence of adaptive immunity. J. Exp. Med. 2012; 209:1869–1882. [PubMed: 22927549]

Orr JS, Puglisi MJ, Ellacott KL, Lumeng CN, Wasserman DH, Hasty AH. Toll-like receptor 4 deficiency promotes the alternative activation of adipose tissue macrophages. Diabetes. 2012; 61:2718–2727. [PubMed: 22751700]

Potian JA, Rafi W, Bhatt K, McBride A, Gause WC, Salgame P. Preexisting helminth infection induces inhibition of innate pulmonary anti-tuberculosis defense by engaging the IL-4 receptor pathway. J Exp Med. 2011; 208:1863–1874. [PubMed: 21825018]

Predina J, Eruslanov E, Judy B, Kapoor V, Cheng G, Wang LC, Sun J, Moon EK, Fridlender ZG, Albelda S, et al. Changes in the local tumor microenvironment in recurrent cancers may explain the failure of vaccines after surgery. Proc. Natl. Acad. USA. 2012; 110:E415–424.

Pyonteck SM, Akkari L, Schuhmacher AJ, Bowman RL, Sevenich L, Quail DF, Olson OC, Quick ML, Huse JT, Teijeiro V, et al. CSF-1R inhibition alters macrophage polarization and blocks glioma progression. Nat Med. 2013; 19:1264–1272. [PubMed: 24056773]

Qian BZ, Pollard JW. Macrophage diversity enhances tumor progression and metastasis. Cell. 2010; 141:39–51. [PubMed: 20371344]

Qiu Y, Nguyen KD, Odegaard JI, Cui X, Tian X, Locksley RM, Palmiter RD, Chawla A. Eosinophils and type 2 cytokine signaling in macrophages orchestrate development of functional beige fat. Cell. 2014; 157:1292–1308. [PubMed: 24906148]

Ries CH, Cannarile MA, Hoves S, Benz J, Wartha K, Runza V, Rey-Giraud F, Pradel LP, Feuerhake F, Klaman I, et al. Targeting tumor-associated macrophages with anti-CSF-1R antibody reveals a strategy for cancer therapy. Cancer Cell. 2014; 25:846–859. [PubMed: 24898549]

Ruffell B, Affara NI, Coussens LM. Differential macrophage programming in the tumor microenvironment. Trends Immunol. 2012; 33:119–126. [PubMed: 22277903]

Sanjabi S, Hoffmann A, Liou HC, Baltimore D, Smale ST. Selective requirement for c-Rel during IL-12 P40 gene induction in macrophages. Proc Natl Acad Sci USA. 2000; 97:12705–12710. [PubMed: 11058167]

Sen R, Smale ST. Selectivity of the NF-[.kappa]B response. Cold Spring Harb Perspect Biol. 2010; 2:a000257. [PubMed: 20452937]

Shand FH, Ueha S, Otsuji M, Koid SS, Shichino S, Tsukui T, Kosugi-Kanaya M, Abe J, Tomura M, Ziogas J, et al. Tracking of intertissue migration reveals the origins of tumor-infiltrating monocytes. Proc Natl Acad Sci USA. 2014; 111:7771–7776. [PubMed: 24825888]

Tundup S, Srivastava L, Nagy T, Harn D. CD14 influences host immune responses and alternative activation of macrophages during Schistosoma mansoni infection. Infect Immun. 2014; 82:3240–3251. [PubMed: 24866794]

Vos AC, Wildenberg ME, Arijs I, Duijvestein M, Verhaar AP, de Hertogh G, Vermeire S, Rutgeerts P, van den Brink GR, Hommes DW. Regulatory macrophages induced by infliximab are involved in healing in vivo and in vitro. Inflamm Bowel Dis. 2012; 18:401–408. [PubMed: 21936028]

Vos AC, Wildenberg ME, Duijvestein M, Verhaar AP, van den Brink GR, Hommes DW. Anti-tumor necrosis factor-alpha antibodies induce regulatory macrophages in an Fc region-dependent manner. Gastroenterology. 2011; 140:221–230. [PubMed: 20955706]

Weisberg SP, McCann D, Desai M, Rosenbaum M, Leibel RL, Ferrante AW Jr. Obesity is associated with macrophage accumulation in adipose tissue. J Clin Invest. 2003; 112:1796–1808. [PubMed: 14679176]

Weiss WA, Aldape K, Mohapatra G, Feuerstein BG, Bishop JM. Targeted expression of MYCN causes neuroblastoma in transgenic mice. EMBO J. 1997; 16:2985–2995. [PubMed: 9214616]

Wynn TA, Chawla A, Pollard JW. Macrophage biology in development, homeostasis and disease. Nature. 2013; 496:445–455. [PubMed: 23619691]

Xu H, Barnes GT, Yang Q, Tan G, Yang D, Chou CJ, Sole J, Nichols A, Ross JS, Tartaglia LA, et al. Chronic inflammation in fat plays a crucial role in the development of obesity-related insulin resistance. J Clin Invest. 2003; 112:1821–1830. [PubMed: 14679177]

Yu M, Zhou H, Zhao J, Xiao N, Roychowdhury S, Schmitt D, Hu B, Ransohoff RM, Harding CV, Hise AG, et al. MyD88-dependent interplay between myeloid and endothelial cells in the initiation and progression of obesity-associated inflammatory diseases. J Exp Med. 2014; 211:887–907. [PubMed: 24752299]

Zhang QW, Liu L, Gong CY, Shi HS, Zeng YH, Wang XZ, Zhao YW, Wei YQ. Prognostic significance of tumor-associated macrophages in solid tumor: a meta-analysis of the literature. PLoS One. 2012; 7:e50946. [PubMed: 23284651]

Zhou L, Nazarian AA, Smale ST. Interleukin-10 inhibits interleukin-12 p40 gene transcription by targeting a late event in the activation pathway. Mol Cell Biol. 2004; 24:2385–2396. [PubMed: 14993278]

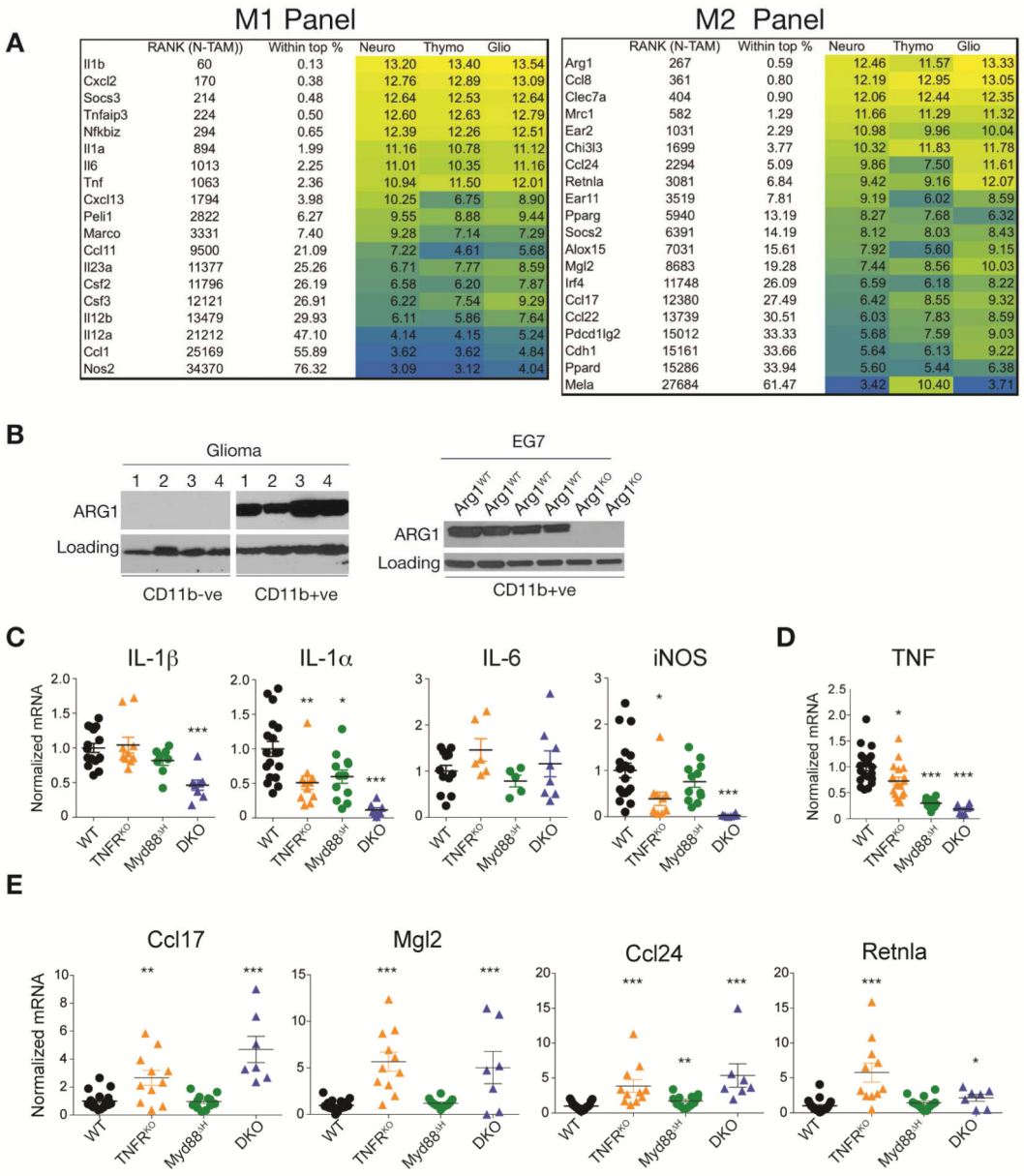

M1 Panel	RANK (N-TAM))	Within top %	Neuro	Thymo	Glio
Il1b	60	0.13	13.20	13.40	13.54
Cxcl2	170	0.38	12.76	12.89	13.09
Socs3	214	0.48	12.64	12.53	12.64
Tnfaip3	224	0.50	12.60	12.63	12.79
Nfkbiz	294	0.65	12.39	12.26	12.51
Il1a	894	1.99	11.16	10.78	11.12
Il6	1013	2.25	11.01	10.35	11.16
Tnf	1063	2.36	10.94	11.50	12.01
Cxcl13	1794	3.98	10.25	6.75	8.90
Peli1	2822	6.27	9.55	8.88	9.44
Marco	3331	7.40	9.28	7.14	7.29
Ccl11	9500	21.09	7.22	4.61	5.68
Il23a	11377	25.26	6.71	7.77	8.59
Csf2	11796	26.19	6.58	6.20	7.87
Csf3	12121	26.91	6.22	7.54	9.29
Il12b	13479	29.93	6.11	5.86	7.64
Il12a	21212	47.10	4.14	4.15	5.24
Ccl1	25169	55.89	3.62	3.62	4.84
Nos2	34370	76.32	3.09	3.12	4.04

M2 Panel	RANK (N-TAM)	Within top %	Neuro	Thymo	Glio
Arg1	267	0.59	12.46	11.57	13.33
Ccl8	361	0.80	12.19	12.95	13.05
Clec7a	404	0.90	12.06	12.44	12.35
Mrc1	582	1.29	11.66	11.29	11.32
Ear2	1031	2.29	10.98	9.96	10.04
Chi3l3	1699	3.77	10.32	11.83	11.78
Ccl24	2294	5.09	9.86	7.50	11.61
Retnla	3081	6.84	9.42	9.16	12.07
Ear11	3519	7.81	9.19	6.02	8.59
Pparg	5940	13.19	8.27	7.68	6.32
Socs2	6391	14.19	8.12	8.03	8.43
Alox15	7031	15.61	7.92	5.60	9.15
Mgl2	8683	19.28	7.44	8.56	10.03
Irf4	11748	26.09	6.59	6.18	8.22
Ccl17	12380	27.49	6.42	8.55	9.32
Ccl22	13739	30.51	6.03	7.83	8.59
Pdcd1lg2	15012	33.33	5.68	7.59	9.03
Cdh1	15161	33.66	5.64	6.13	9.22
Ppard	15286	33.94	5.60	5.44	6.38
Mela	27684	61.47	3.42	10.40	3.71

Figure 1. Cooperative MyD88-TNF signaling drives expression of M1/M2 genes in TAMs

(A) M1 and M2 associated gene expression in TAMs isolated from 3 tumor models (Neuroblastoma: Neuro; Tymoma: Thymo; Glioma: Glio) and analyzed by microarray. Signal intensities are shown with the rank among 45037 probe sets (in N-TAMs). Color code represents high (yellow) to low (blue) intensities. Data are representative of the $\log_2$ signal intensities (n = 3 per TAM type). **(B)** Immunoblot analysis of ARG1 expression in $CD11b^+$ and $CD11b^-$ fractions isolated from EG7 thymomas or gliomas grown in *Arg1*$^{flox/flox}$;Tie2-cre ($Arg1^{KO}$) and WT (*Arg1*$^{flox/flox}$ littermates) mice. **(C, D** and **E)** qRT-PCR of EG7 TAM RNA isolated from WT, $TNFR^{KO}$, *Myd88*$^{\Delta H}$ or DKO mice. Each dot represents the expression values from individual mice from at least 2 experiments with the black line representing the mean. Error bars, SEM. Statistical significance was calculated using two-tailed Student's t test and is indicated by *p< 0.05, **p< 0.01, ***p< 0.001.

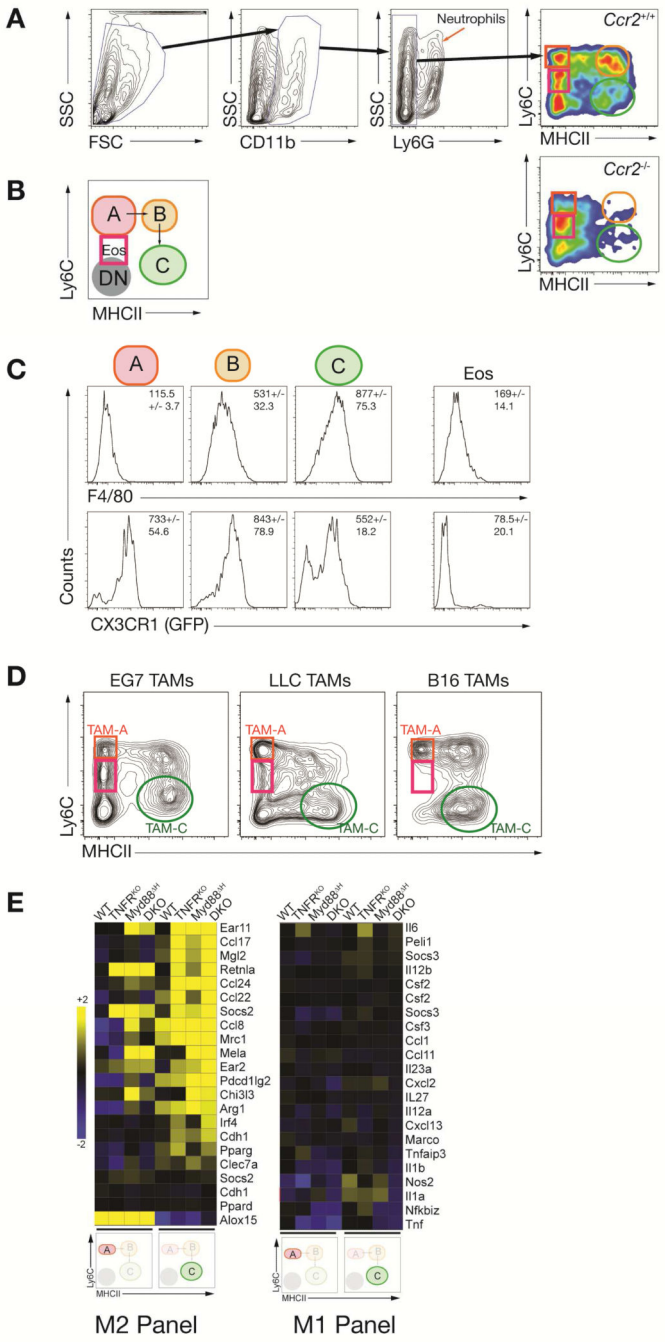

Figure 2. MyD88 and TNFR1 signaling suppress M2 gene expression in TAMs

(A) Gating strategy of TAM populations A (red ellipse), B (orange ellipse) and C (green ellipse) as well as tumor-infiltrating eosinophils (Eos, purple square) and double negative (DN) cells for sorting experiments comparing EG7 TAMs from WT and *Ccr2*$^{-/-}$ mice. **(B)** Schematic representation of TAM development from TAM-A to TAM-C. **(C)** F4/80 and CX3CR1-GFP expression in EG7 TAMs isolated from WT and CX3CR1-GFP mice in TAM fractions as shown in **A** and **B**. Data are representative histograms of 3 (F4/80; n = 10) or 1 (CX3CR1-GFP; n = 3) experiments. **(D)** TAM fractions in macrophages gated as shown

in **A** isolated from different transplantable tumor models. Blots are representative for at least 2 experiments where each experiment used at least 5 mice per tumor type. **(E)** Transcriptome analysis of EG7 TAM populations A and C derived from WT, $TNFR^{KO}$, $Myd88^{\Delta H}$ or DKO mice. Depicted values of M1 and M2 associated genes are heat maps arranged by $\log_2$ signal intensities (n = 2 per genotype).

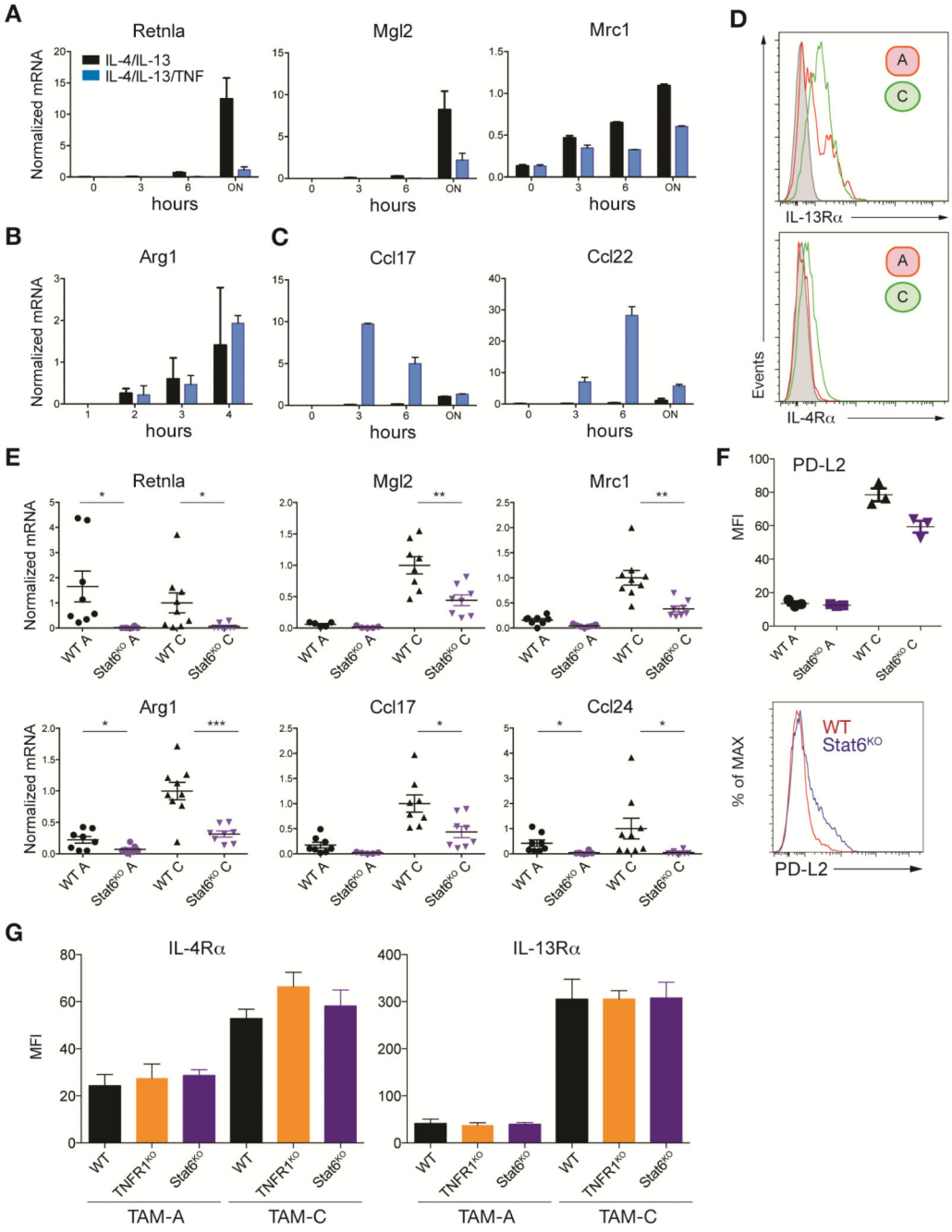

Figure 3. TNF signaling blocks IL-13 derived M2 polarization

(A-C) qRT-PCR analysis of BMDMs left unstimulated or treated with a cocktail of IL-4 and IL-13 in combination with or without TNF for the times indicated. Data are the mean expression values (n = 2) and are representative for 1 out of 2 experiments. **(D)** Flow histograms of IL-4Rα and IL-13Rα expression in EG7 TAM populations A and C, representative of 2 experiments (n = 10). Unstained control is shown in grey. **(E)** qRT-PCR of M2 genes EG7 TAM populations A and C isolated from WT and Stat6^{KO} mice. Data are the expression values from individual mice (n ≥ 7) from 2 experiments with the black line

representing the mean. **(F)** The expression of the M2 marker PD-L2 in EG7 TAM populations A and C was analyzed by flow cytometry isolated from WT and $Stat6^{KO}$ mice. Data are shown as Median Fluorescence Intensity (MFI) (n = 3) and representative flow analysis in TAM-C. **(G)** IL-4Rα and IL-13Rα expression in EG7 TAM populations A and C analyzed by flow cytometry as shown in **(D)** isolated from WT, $TNFR^{KO}$ and $Stat6^{KO}$ mice. Data are shown as Median Fluorescence Intensity (MFI) (WT, $Stat6^{KO}$: n = 4; $TNFR^{KO}$: n = 3) and represent 1 out of 3 experiments. Statistical significance was calculated using a two-tailed Student's t test and is indicated by *p< 0.05, **p< 0.01, ***p< 0.001. Error bars, SEM.

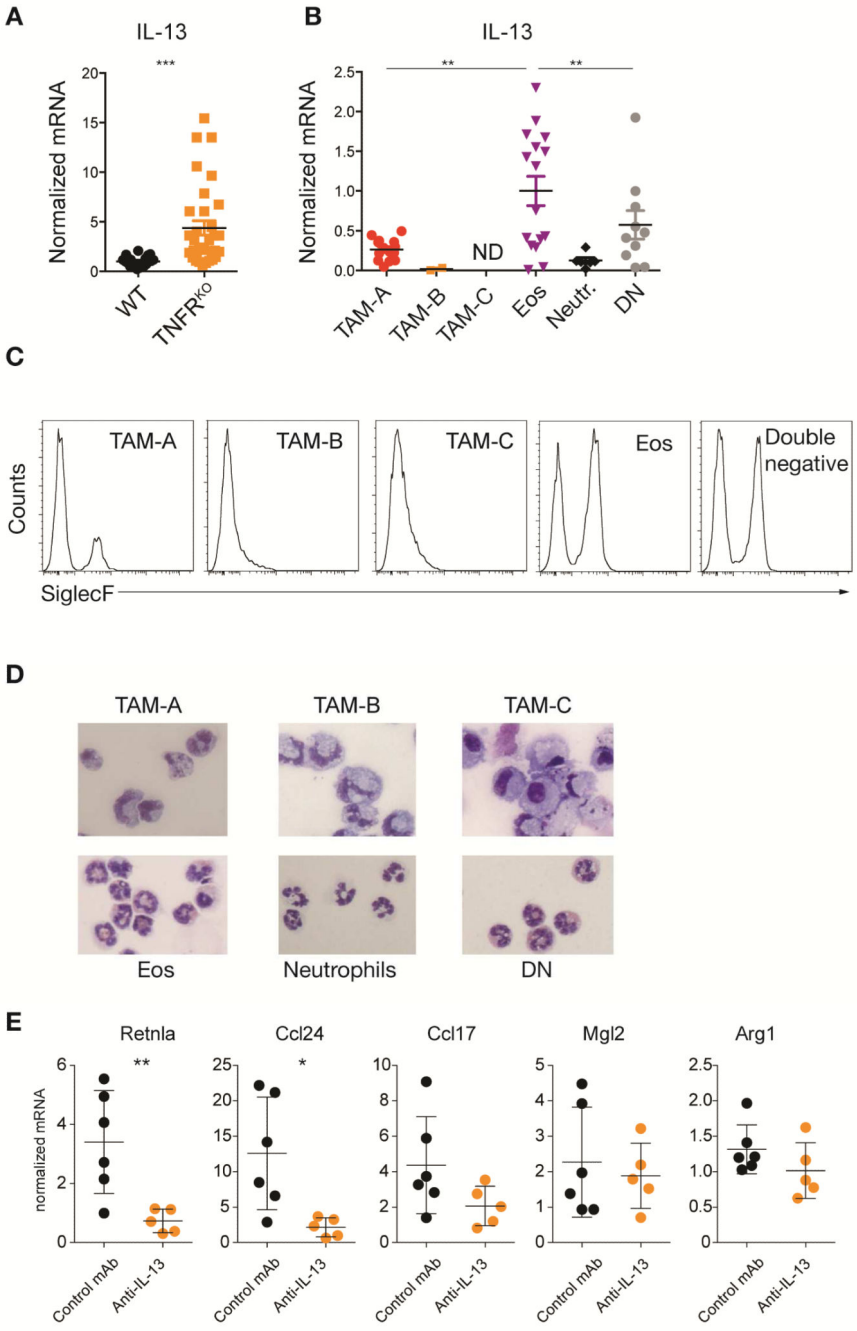

Figure 4. Tumor infiltrating eosinophil derived IL-13 drives M2 expression in TAMs

(A and B) qRT-PCR analysis of IL-13 production in EG7 TAM unsorted (**A**) or sorted for TAM subpopulations as depicted in Figure 2A and B. Values from individual mice (**A:** n ≥ 21; **B:** n ≥ 10) from at least 2 experiments are shown. Data in **B** were normalized to eosinophils (Eos). Error bars, SEM. **(C)** SiglecF expression analyzed by flow cytometry in TAM subpopulations gated as shown in Figure 2. Plots are representative for 3 experiments. **(D)** H&E stained cytospin slides of EG7 TAM populations (40× magnification). Pictures shown are representative of 2 experiments (n = 4). **(E)** qRT-PCR analysis of $CD11b^{+}$ EG7

TAMs derived from control IgG1 or anti-IL-13 antibody treated $TNFR^{KO}$ mice ($n \geq 5$). Mean expression values from 1 of 2 experiments are shown. Error bars, SEM. Statistical significance was calculated using a One-way Anova **(B)** or two-tailed Student's t test **(A and E)** and is indicated by *p< 0.05, **p< 0.01, ***p< 0.001.

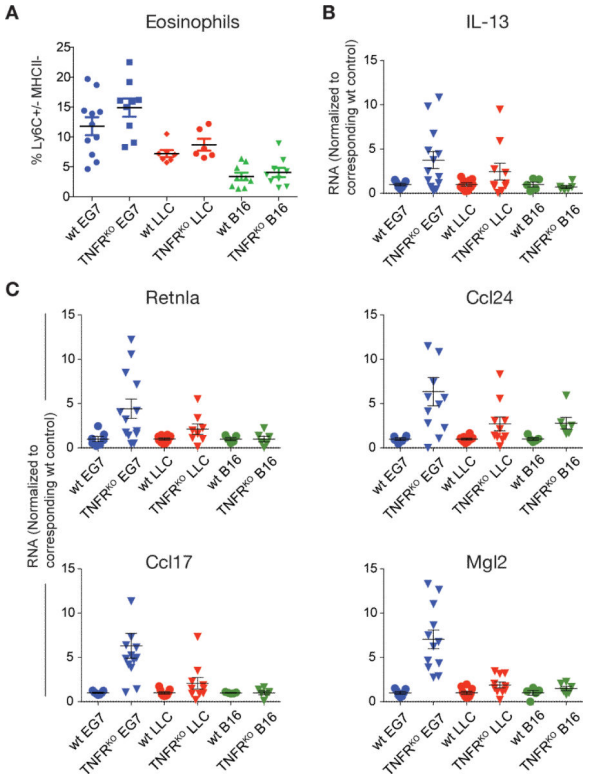

Figure 5. M2 gene expression in TNFR^{KO} TAMs correlates with tumor infiltrating eosinophils

(A) Frequency of tumor infiltrating eosinophils in 3 different tumor models (EG7, LLC and B16) in WT and TNFR^{KO} mice gated as in Figure 2A. Data are values from individual mice ($n \geq 6$) from at least 2 independent experiments per tumor model. Cell frequencies are shown as % Ly6C$^{+/-}$ MHCII^{-} cells of all CD11b^{+}Ly6G^{-} cells. Error bars, SEM. **(B and C)** qRT-PCR analysis of CD11b^{+} TAMs isolated from different tumor models in WT and TNFR^{KO} mice as in **A** ($n \geq 5$). Data are the mean expression values normalized to the corresponding WT TAMs in each tumor model and represent values from individual mice from at least 2 independent experiments per tumor model. Error bars, SEM.

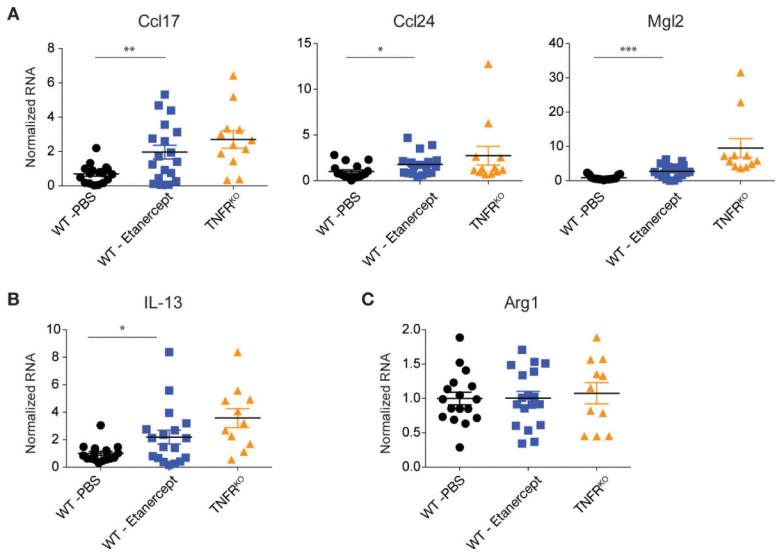

Figure 6. Treatment with the anti-TNF drug Etanercept enhances IL-13 and M2-associated gene expression in TAMs

(A, B and C) qRT-PCR analysis of CD11b^{+} EG7 TAMs isolated from PBS (n ≥ 17) or Etanercept (n ≥ 18) treated WT mice compared to TAMs from TNFR^{KO} mice (n ≥ 11). Data represent individual mice from 3 experiments normalized to the corresponding mean PBS treated WT TAMs per experiment. Error bars, SEM. Statistical significance was calculated using a two-tailed Student's t test and is indicated by *p< 0.05, **p< 0.01, ***p< 0.001. Error bars, SEM.